Climate anomalies contributed to the rebound of PM2.5 in winter 2018 under intensified regional air pollution preventions

Article *in* Science of The Total Environment · July 2020

DOI: 10.1016/j.scitotenv.2020.138514

CITATIONS
5

READS
10

2 authors, including:

Zhicong Yin
Nanjing University of Science and Technology
39 PUBLICATIONS **365** CITATIONS

SEE PROFILE

Science of the Total Environment 726 (2020) 138514

Contents lists available at ScienceDirect

Science of the Total Environment

journal homepage: www.elsevier.com/locate/scitotenv

Climate anomalies contributed to the rebound of $PM_{2.5}$ in winter 2018 under intensified regional air pollution preventions

Zhicong Yin [a,b,c,*], Yijia Zhang [a]

[a] Key Laboratory of Meteorological Disaster, Ministry of Education/Joint International Research Laboratory of Climate and Environment Change (ILCEC)/Collaborative Innovation Centre on Forecast and Evaluation of Meteorological Disasters (CIC-FEMD), Nanjing University of Information Science & Technology, Nanjing 210044, China
[b] Southern Marine Science and Engineering Guangdong Laboratory (Zhuhai), Zhuhai, China
[c] Nansen-Zhu International Research Centre, Institute of Atmospheric Physics, Chinese Academy of Sciences, Beijing, China

HIGHLIGHTS

- Under intensified regional air pollution preventions, the haze pollution dramatically rebounded in the winter of 2018.
- Both of the observed analyses and the GEOS-Chem results demonstrated the effect of climate anomalies on the rebound in 2018.
- The teleconnection patterns related to external factors were comprehensively conductive to the $PM_{2.5}$ rebound.

GRAPHICAL ABSTRACT

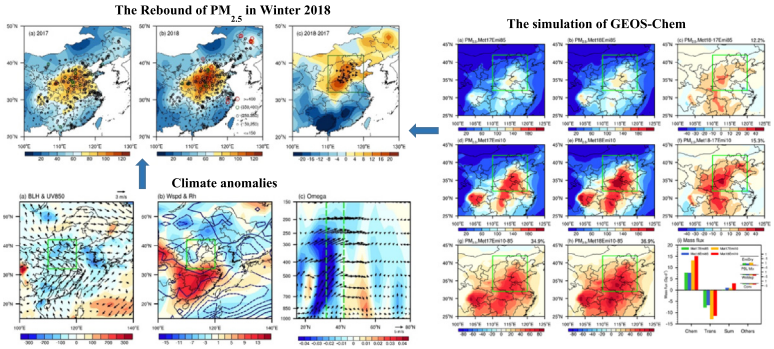

ARTICLE INFO

Article history:
Received 15 March 2020
Received in revised form 3 April 2020
Accepted 5 April 2020
Available online 19 April 2020

Editor: Jianmin Chen

Keywords:
Air pollution
Atmospheric teleconnection
$PM_{2.5}$
Emission reduction

ABSTRACT

Rigorous air pollution managements since 2013 resulted in decreasing trend in fine particulate matter ($PM_{2.5}$) in China. Regional air pollution prevention measures were extra implemented in the "2 + 26" region since 2017. However, haze pollution dramatically rebounded in the winter of 2018. Both of the observed analyses and the numerical results (basing on a global 3-D chemical transport model) demonstrated that, although intensified prevention measures existed, atmospheric circulation and local meteorological conditions still significantly influenced the variation in haze pollution. The simulated $PM_{2.5}$ concentrations (with fixed emissions) driven by meteorology in 2018 were 12–15% higher than those with atmospheric circulations in 2017 both under a low and a high emission level, close to the observed 10% $PM_{2.5}$ rebound. In 2018, positive sea ice anomalies around Beaufort Sea and "triple pattern" anomalies of sea surface temperature in the North Pacific and North Atlantic enhanced the anomalous anticyclonic circulations over the air-polluted region, and thus resulted in minimum surface wind speed during 1979–2018 and 16.8% shallower boundary layer than those in 2017. In the stagnated air of winter 2018, the transported dispersion of pollutant particles was weakened, however more secondary aerosols were produced by enhanced chemical reactions, which jointly contributed to the $PM_{2.5}$ rebound in 2018.

* Corresponding author at: Key Laboratory of Meteorological Disaster, Ministry of Education/Joint International Research Laboratory of Climate and Environment Change (ILCEC)/Collaborative Innovation Centre on Forecast and Evaluation of Meteorological Disasters (CIC-FEMD), Nanjing University of Information Science & Technology, Nanjing 210044, China.
E-mail address: yinzhc@163.com (Z. Yin).

https://doi.org/10.1016/j.scitotenv.2020.138514
0048-9697/

1. Introduction

Haze pollution, with low visibility and high concentration of fine particulate matter ($PM_{2.5}$), dramatically endangers human health, ecological sustainability and economic development. After a severe haze event in the Beijing-Tianjin-Hebei region in January 2013, series of air quality protection policies were published, mainly including shutting down polluting factories and restricting fuel vehicles (Wang, 2018). Although the annual mean $PM_{2.5}$ concentrations have been reduced in several polluted cities (Li et al., 2019), severe winter haze episodes still frequently occurred (Yin et al., 2019). For example, during December 16th–21st 2016, severe haze pollution with $PM_{2.5}$ concentrations of 1100 μg m^{-3} occurred and covered 710,000 km^2 (Yin and Wang, 2017). In addition to local emissions, regional transportation was a major source of air pollution (An et al., 2019); thus, regional prevention and treatments should be more effective in reducing $PM_{2.5}$ concentrations. In 2017, the "2017 Air Pollution Prevention and Management Plan for the Beijing-Tianjin-Hebei Region and its Surrounding Areas" was released to direct the "2 + 26" cities to jointly resolve their air pollution issues (Ministry of Environmental Protection of China, 2017). These "2 + 26" cities (Fig. 1c) are mainly located in the most polluted areas of North China (2 + 26 region: 32–42°N, 110–120°E). Chen et al. (2019) summarized the effects of the "2 + 26" regional strategy and found a 32.7% decrease in mean $PM_{2.5}$ concentrations in November 2017 compared with those in November 2016 which were attributed to local emissions limitations; however, large-scale atmospheric circulations and local meteorological effects were not considered.

Climate and weather conditions contributed to the variations in haze pollution in China (Yin et al., 2015; An et al., 2019). Numerical simulations, by a global 3-D chemical transport model (GEOS-Chem), quantitatively illustrated that the interannual-decadal variations in haze pollutions were mostly attributive to the climate variability (Dang and Liao, 2019; Li et al., 2019). By modulating local meteorological conditions, the autumn Arctic sea ice (Wang et al., 2015; Yin et al., 2019) and preceding sea surface temperature (SST) anomalies (Yin and Wang, 2016; Xiao et al., 2015) played important roles in the development of severe haze in North China in 2014 (Yin et al., 2017). The positive anomalies of snow in western Siberia induced the East Atlantic/West Russia (EA/WR) pattern to influence severe haze in December in 2016 (Yin and Wang, 2017). The Antarctic Oscillation was an influential

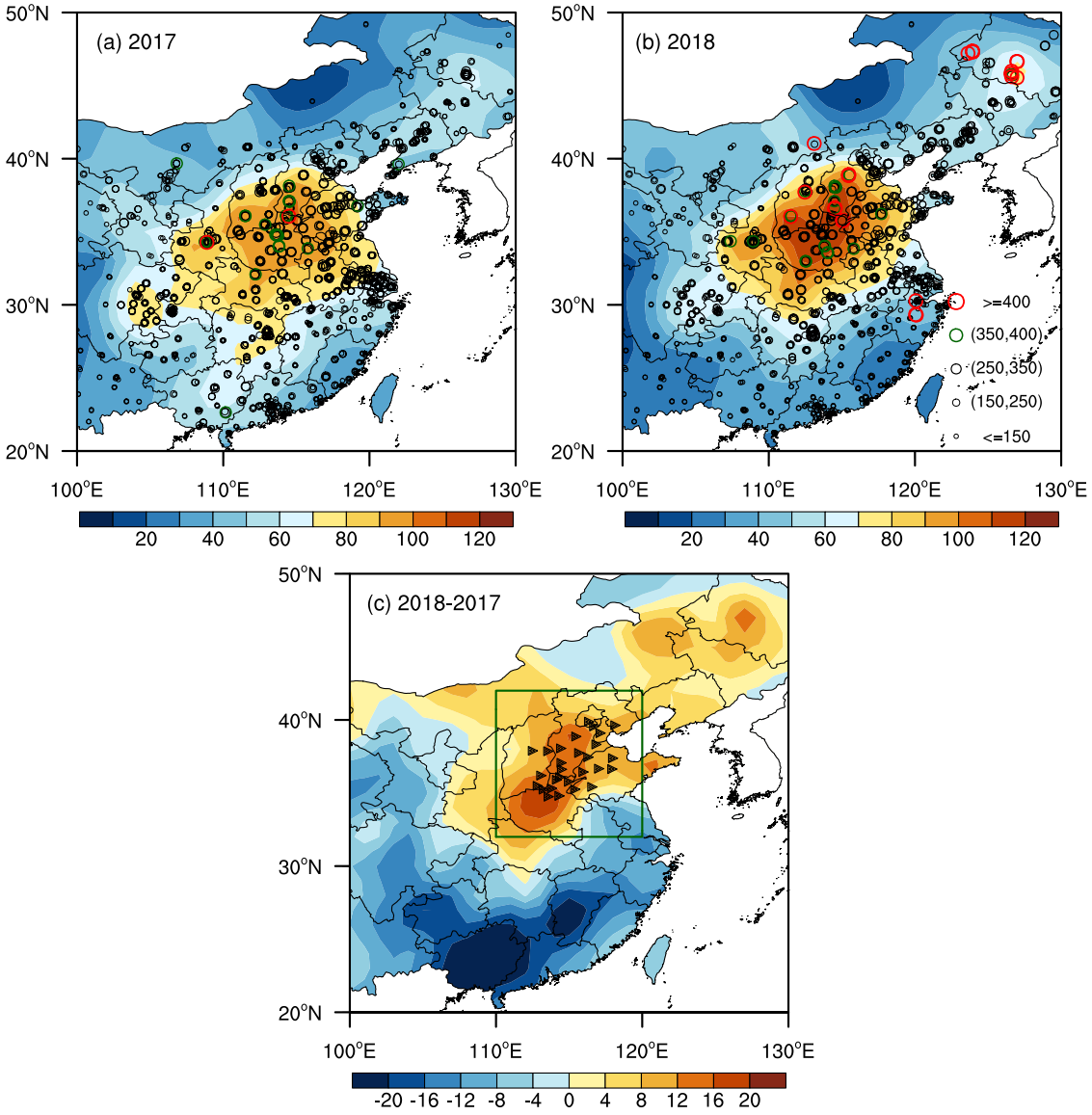

Fig. 1. Distribution of $PM_{2.5}$ concentrations (unit: μg m^{-3}): means (shading) and daily maximums (hollow circle) $PM_{2.5}$ for the winters of 2017 (a) and 2018 (b), and differences in the winter means of $PM_{2.5}$ between 2017 and 2018 (c). The triangles in panel c indicate the "2 + 26" cities in the regional strategy for air quality improvement, while the rectangle represents the 2 + 26 region (32–42°N, 110–120°E).

factor, showing significant negative correlation with North China haze pollution (Zhang et al., 2019) and exerting its impact on local dispersion conditions. The EA/WR, West Pacific and Eurasia (EU) patterns were proved to be effective atmospheric bridges linking distant and preceding climate signals to local anomalous anticyclonic circulations over Northeast Asia (Yin et al., 2017), i.e., the main local atmospheric circulations related to North China haze pollution (Zhong et al., 2019). In 2013 and 2014, the frequency of cold air was lower than that in the other years during 2010–2017, resulting in more haze pollution in Beijing (He et al., 2018). Locally, slow surface winds (Shi et al., 2019), a lower boundary layer and high relative humidity result in stagnant air, which limits the dispersion of particulates (Chen and Wang, 2015).

In the winters of 2017 and 2018, regional air pollution prevention measures were implemented and largely limited the levels of anthropogenic emissions, however, it was evident that the 2 + 26 region was still the most severely polluted area in China (Fig. 1). Significant differences in $PM_{2.5}$ concentrations were observed during these 2 years (Fig. 1c). The winter mean $PM_{2.5}$ concentrations in 2017 were approximately 60–90 μg m^{-3}, while means in the following year were 70–110 μg m^{-3}. This raised a question: what are the reasons for these noteworthy differences in $PM_{2.5}$ concentrations between two adjacent years under the same regional strategy for air quality improvement? Are there any implications for emission reductions? In this study, we attempt to discern climate causes for the observed rebound in $PM_{2.5}$ concentrations under decreasing tendency.

2. Data sets and methods

2.1. Data descriptions

In this study, the daily meteorological data and $PM_{2.5}$ observations in 2017–2018 were used to analyse the status of haze pollution and reveal the impacts of climate differences. Furthermore, the long sequences of meteorological data from 1979 to 2019 were also employed to illustrate long-standing linkages between the number of haze days and climate anomalies, which provided robust basis for the diagnosis of $PM_{2.5}$ rebound in 2018.

Daily $PM_{2.5}$ concentrations were observed by 1504 sites in East China (Fig. 1a) and were downloaded from a public database (http://beijingair.sinaapp.com/), widely used in studies related to Chinese air pollution issues. The mean $PM_{2.5}$ concentration of the 2 + 26 region is the average of 398 stations over this area. In addition to $PM_{2.5}$ concentrations, the number of haze days were also important factors to measure the levels of haze pollutions, which came from the haze definitions in atmospheric science and overcame the limited length of $PM_{2.5}$ observations. The number of haze days was calculated from the long-term meteorological data during 1979–2019, mainly based on observed visibility and relative humidity (Yin et al., 2017).

The daily meteorological data for the winters of 2017 and 2018, and monthly mean meteorological data from 1979 to 2019 were obtained from NCEP/NCAR reanalysis datasets, with a horizontal resolution of 2.5° × 2.5°. The variables included geopotential heights at 500 hPa (H500), zonal and meridional winds at 200 hPa, 850 hPa and the surface, vertical winds from surface to 150 hPa, surface air temperatures (SAT), sea level pressures (SLP), and relative humidity from surface to 300 hPa (Kalnay et al., 1996). The boundary layer height (BLH, 1° × 1°) values were from Interim reanalysis data (ERA-Interim) obtained from the European Centre for Medium-Range Weather Forecasts (ECMWF) (Dee et al., 2011). The monthly precipitation data used in this study were from the CPC Merged Analysis of Precipitation data (CMAP, 2.5° × 2.5°) obtained from the National Oceanic and Atmospheric Administration (Smith et al., 2008). The monthly sea ice concentrations (1° × 1°) were downloaded from the Met Office Hadley Centre (Rayner et al., 2003). The monthly mean extended reconstructed SST datasets (2° × 2°) were obtained from the National Oceanic and Atmospheric Administration (Smith et al., 2008).

2.2. GEOS-Chem description and experiment designs

The $PM_{2.5}$ concentrations were also produced by GEOS-Chem model (http://acmg.seas.harvard.edu/geos/). The GEOS-Chem model was driven by MERRA-2 assimilated meteorological data (Gelaro et al., 2017). The nested-grid over China (15°S–55°N, 75–135°E) was with a horizontal resolution of 0.5° latitude by 0.625° longitude and 47 vertical layers up to 0.01 hPa. The GEOS-Chem model includes fully coupled O_3-NO*x*-hydrocarbon and aerosol chemistry with >80 species and 300 reactions (Bey et al., 2001; Park et al., 2004). According to Dang and Liao (2019), we calculated the simulated $PM_{2.5}$ concentrations in this study as the sum of the mass of sulfate, nitrate, ammonium, black carbon and organic carbon. Concentrations of $PM_{2.5}$ are jointly determined by emissions, transport, chemical reactions, and deposition. For each component, seven processes physical-chemical process jointly determined the mass balance of aerosols (i.e., mass fluxes of aerosols), including emissions, chemistry, convection, dry deposition, wet deposition, PBL mixing, transport. In this study, the physical-chemical process analysis was executed for the "2 + 26" region and within the planetary boundary layer.

Daily $PM_{2.5}$ concentrations in the winters of 2017 and 2018 were simulated in this study. Due to delayed updates of emission inventory, we did not aim to design numerical experiments to reproduce the observations in 2017 and 2018. Here, we used the emissions data in 1985 and 2010 (Fig. S1a, b), which were downloaded from the website of GEOS-Chem (http://geoschemdata.computecanada.ca/ExtData/HEMCO/AnnualScalar). The emissions in 1985 and 2010 were largely different and could represented a low emission scenario and a high emission scenario (Fig. S1c). Totally, there were 4 numerical experiments according to different combinations of meteorological conditions and emissions which drive the GEOS-Chem simulations.

Met17Emi85: the GEOS-Chem model were driven by meteorological fields in winter 2017 and emissions in winter 1985;

Met18Emi85: the GEOS-Chem model were driven by meteorological fields in winter 2018 and emissions in winter 1985;

Met17Emi10: the GEOS-Chem model were driven by meteorological fields in winter 2017 and emissions in winter 2010;

Met18Emi10: the GEOS-Chem model were driven by meteorological fields in winter 2018 and emissions in winter 2010;

3. Impacts of meteorological anomalies

The differences in winter mean $PM_{2.5}$ concentrations between 2018 and 2017 yielded opposite signs for North and South China (Fig. 1c). From Guangxi to Jiangxi Provinces, $PM_{2.5}$ concentrations were much lower in the winter of 2018 than the corresponding measurements in 2017; however, in North China, the winter mean $PM_{2.5}$ concentrations in 2018 were higher than those in 2017. The negative anomalies in South China might related to sufficient precipitation in winter of 2018, which brought about strong wet deposition (Fig. S2b). In this study, we focused on the most polluted area in China (2 + 26 region), where the $PM_{2.5}$ concentrations was 71.9 and 78.7 μg m^{-3} in 2017 and 2018, respectively. The differences in these 2 years accounted for approximately 10% of the actual concentration in the 2 + 26 region. In addition to winter mean $PM_{2.5}$ concentrations, the number of severe haze-polluted days (area-mean $PM_{2.5}$ concentration > 100 μg m^{-3}) was 23.1% higher in 2018 (32 days) than in 2017 (26 days). The number of sites with maximum daily $PM_{2.5}$ > 350 μg m^{-3} were 23 in 2017 in the 2 + 26 region (Fig. 1a), however, the numbers increased up to 37 in 2018 (Fig. 1b), with growth rate = 60.9%. Therefore, both the intensity and coverage of haze pollutions rebounded in the winter of 2018.

Low surface wind speeds and weak cold air resulted in bad horizontal ventilation (Ma et al., 2017). A strong thermal inversion layer and lower BLH meant that fine particles accumulated in a shallower layer and could not disperse (Liu et al., 2018). High surface humidity provided

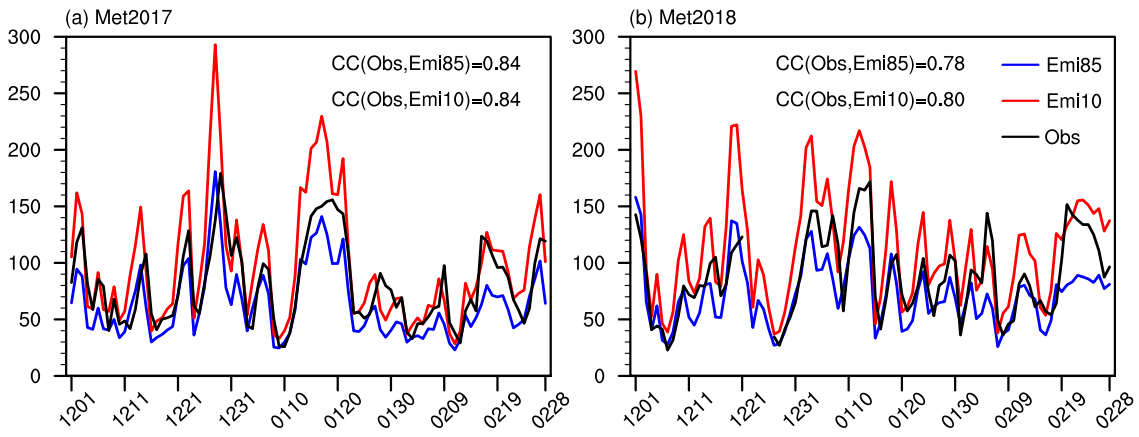

Fig. 2. Area-mean daily $PM_{2.5}$ concentrations (unit: μg m^{-3}) in winter of 2017 (a) and 2018 (b) from observations (black), numerical simulation under emission in 1985 (blue) and numerical simulations under emissions in 2010 (red).

a favourable environment for hygroscopic growth of pollutant particles (Ding and Liu, 2014). Thus, we regressed the daily $PM_{2.5}$ concentrations with the BLH, surface wind speed, SAT and humidity. The daily variations and values of $PM_{2.5}$ were well reproduced (Figure omitted), with correlation coefficient at a confidence level of 99% both in 2017 (0.72) and 2018 (0.67). With fixed emissions, the GEOS-Chem model also successfully reproduces the daily variations in $PM_{2.5}$ concentrations. That is, the correlation coefficients between daily observed and simulated $PM_{2.5}$ concentrations were 0.84 (Met17Emi85), 0.84 (Met17Emi10), 0.78 (Met18Emi85) and 0.80 (Met18Emi10), which were above 99% confidence level and indicated that the daily variation in meteorological conditions dominated the daily fluctuations of haze pollutions (Fig. 2). The strong synoptic correlations provided robust basis for the following climate analysis.

With regard to winter means, an anticyclonic anomaly existed over North China and the Japan Sea, inducing anomalous southerly winds at 850 hPa (Fig. 3a). These anomalous southerlies could be traced to the South China Sea, transported moisture and converged over the middle and lower Yangtze River. This was one of the possible reasons for greater precipitation in this location during the winter of 2018 (Fig. S2d). On the other hand, these southerlies weakened the East Asia winter monsoon. That is, the surface wind speeds in the 2 + 26 region were slowed, meaning that horizontal ventilation conditions were worse in 2018 than in 2017 (Fig. 3b). From 20°N to 40°N, tilted ascending motion was observed (Fig. 3c), resulting in favourable conditions for precipitation to the south of 30°N and limiting the downward transport of westerly momentum at mid and upper levels over the 2 + 26 region. The weak downward westerly momentum reduced the cold air near the surface and lowered the surface wind speed (Zhong et al., 2019). Winter BLH in 2018 was lower than in 2017 and the centre of their differences was located in the Beijing-Tianjin-Hebei region (Fig. 3a). Quantitatively, the area-averaged BLH was 486 *m* in winter 2017, 16.8% higher than in 2018 (Fig. 4; Table S1). The surface wind speeds in 2017 (3.4 m/s) were 17.2% greater than those in 2018 (2.9 m/s). Horizontal and vertical dispersion conditions were both better in 2017 than in 2018. It is worth noting that the moisture conditions in 2018 were similar to those in 2017, thus the conditions for hygroscopic growth were not the reason for the $PM_{2.5}$ differences in these 2 years (Fig. 4; Table S1). Furthermore, the surface wind speeds at a minimum in 2018, corresponding to the worst horizontal dispersions during 1979–2018. Joint with lower BLH, the $PM_{2.5}$ rebound in 2018 under the deceasing trend. In contrast, the BLH in 2017 was the highest during 1979–2018 indicating best vertical dispersion (Fig. 4). The surface wind speed in 2017 was largest in the recent decade. The meteorological conditions in winter 2017 led to good air quality, which enlarged the decreasing tendency of $PM_{2.5}$ and overplayed the effects of emission reductions.

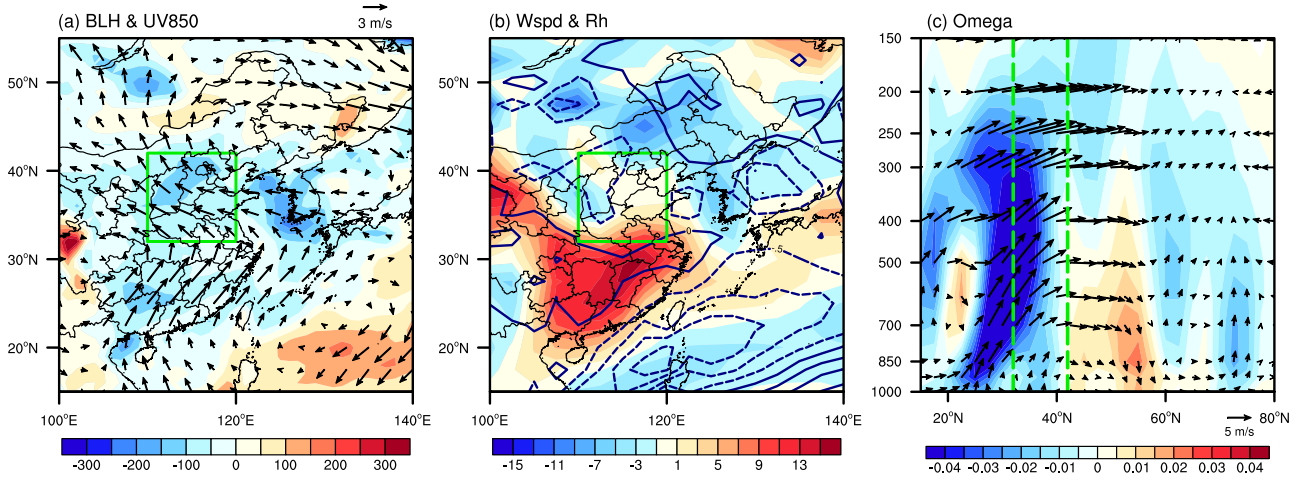

Fig. 3. Differences in winter (a) BLH (shading, unit: m), wind at 850 hPa (arrows, unit: m/s) and (b) surface relative humidity (shading, unit: %), surface wind speed (contour, unit: m/s) between 2018 and 2017 (2018 minus 2017). Differences in (c) 112–118°E mean vertical motion (arrows, unit: m/s) and omega (shading, unit: pascal/s) between winters in 2018 and 2017 (2018 minus 2017). The linear trend was removed. The green box in panel a-b is the location of the 2 + 26 region, and the green lines in panel c indicate the latitudes of the 2 + 26 region.

4. Quantifying the meteorological impacts via GEOS-Chem model

During the observational analyses, we assumed that similar regional air pollution preventions in two adjacent years resulted in almost the same emissions, however, we could not fully exclude the influences of the small differences of anthropogenic emissions to the rebound of haze pollution in winter 2018. Thus, to confirm the impacts of meteorological conditions, numerical experiments using GEOS-Chem were carried out by comparing the simulated $PM_{2.5}$ under different atmospheric circulations in 2017 and 2018 but with fixed emissions. That is, the differences of $PM_{2.5}$ between Met17Emi85 and Met18Emi85 and those between Met17Emi10 and Met18Emi10 were considered to isolate the roles of meteorological conditions. In these two comparisons, the impacts of meteorological conditions could be assessed both under a low and a high emission level. The GEOS-Chem model was widely used in the studies on air pollutions in China basing on its good performances to reproduce the observed atmospheric components (Li et al., 2019; Feng et al., 2019). Furthermore, Dang and Liao (2019) applied the GEOS-Chem model to prove that the interannual-decadal variations of haze cannot be reproduced when the simulations were solely driven by varying emissions (i.e., the meteorological conditions were fixed), but can be reproduced with varying meteorological conditions and fixed emissions. It was evident that all of four simulations successfully reproduced spatial distributions of the most polluted areas in China, e.g., Beijing-Tianjin-Hebei, Fenwei Plain, Sichuan Basin and Yangtze River Delta (Fig. 5a, b, d and e). As a new defined polluted region, the 2 + 26 region covered most of North China (including Beijing-Tianjin-Hebei) and Fenwei Plain. Therefore, it is reasonable to discuss the reasons for the differences of haze pollutions in the 2 + 26 region via the aforementioned GEOS-Chem simulations.

The centres of the $PM_{2.5}$ differences were located near the 2 + 26 regions and distributed from the southwest (Henan Province) to the northeast (Hebei Province) under two different emissions (Fig. 5c, f), which was similar to the distribution of the observed differences (Fig. 1c). As expected, under the same levels of emissions, the meteorological conditions in winter 2018 certainly resulted in higher $PM_{2.5}$ concentrations in the 2 + 26 region than in 2017 (Fig. 5a–f). The winter-mean $PM_{2.5}$ concentrations in the 2 + 26 region were 64.1 (Met17Emi85), 72.4 (Met18Emi85), 98.4 (Met17Emi10) and 114.7 (Met18Emi10) μg m^{-3}. Although the absolute differences of area-mean $PM_{2.5}$ between 2018 and 2017 seemingly differed greatly, the percentage (the differences / mean concentration) was 12.2% (under emission in 1985, Fig. 5c) and 15.3% (under emission in 2010, Fig. 5f) that was close to the observations (10%). The number of days with $PM_{2.5} < 75$ μg m^{-3} and $PM_{2.5} > 125$ μg m^{-3} were also counted (Table S2). When the GEOS-Chem model was driven by the emissions in 2010, the number of severe haze days increased about 54% in 2018 (37 days) comparing to those in 2017 (22 days), however, the number of days with $PM_{2.5} < 75$ μg m^{-3} declined nearly 53% (22 days in 2018 and 38 days in 2017). These percentages under 1985 emissions were smaller, but the meteorological conditions in 2018 also resulted in a larger number of severe haze days and less days with good air quality than those in 2017 (Table S2).

Mass balance of $PM_{2.5}$ are jointly determined by seven processes (i.e., emissions, chemistry reaction, convection, dry deposition, wet deposition, PBL mixing and transport) which could be isolated by the GEOS-Chem model. As shown in Fig. 5i, the effect of emission and dry deposition was summed up in this numerical model, which was a small value (relative to chemistry reaction and transport) as well as convection, wet deposition and PBL mixing (Dang and Liao, 2019). Here, we focused on the total effects of seven processes, and the roles of chemistry reaction and transport. When the emissions were low (i.e., Met17Emis85 and Met18Emis85), the positive contributions of chemical reactions were also low (~7.5 Gg d^{-1}) and almost unchanged with the meteorological conditions (Fig. 5i). However, under high emissions, the chemical reactions increased 15.3% in 2018 (15.1 Gg d^{-1}) comparing to those in 2017 (13.1 Gg d^{-1}), indicating that the bad dispersion conditions actually enhanced the chemical reactions in the atmosphere to produce more secondary aerosols. The transport of aerosols exported the particles to the downwind areas as well as to the upper troposphere. The contributions of transport were sensitive to the change of meteorology conditions (Fig. 5i). During the atmospheric circulations in 2018, the outflow of pollutant particles decreased greatly, 13.3% and 11% under low and high emissions respectively. Thus, the stagnated air in 2018 weakened the transport process but enhanced the chemical reactions, and thus held more particles in 2 + 26 region. As regard to the joint contributions of transport and chemical reactions, the budget due to changes in atmospheric circulations were 0.96 Gg d^{-1} (1985 emission level) and 3.31 Gg d^{-1} (2010 emission level). When the stagnated meteorology (dispersed atmosphere) and high emissions met, the total effects of seven processes had a value with 3 (0.73) Gg d^{-1} (Fig. 5i). Therefore, the results of GEOS-Chem simulations confirmed that changes in meteorological conditions strongly contributed to the differences of $PM_{2.5}$ in the winter 2017 and 2018.

5. Linkages with preceding SST and ASI

Large-scale atmospheric circulation provided a background for changes in local meteorological conditions associated with haze pollution. Differences in geopotential height at 500 hPa were composited to explore the signals of large-scale atmospheric circulation. There were alternately positive and negative H500 anomalies over the central-north Atlantic (+), west Europe (−), the north eastern Caspian Sea and North China (+). This positive phase of EA/WR enhanced the anticyclonic circulations over North China and intensified haze pollution in the 2 + 26 region (Yin et al., 2017). The negative H500 anomalies over the polar region and positive anomalies over North China formed the positive phase of EU teleconnection pattern and contributed to the

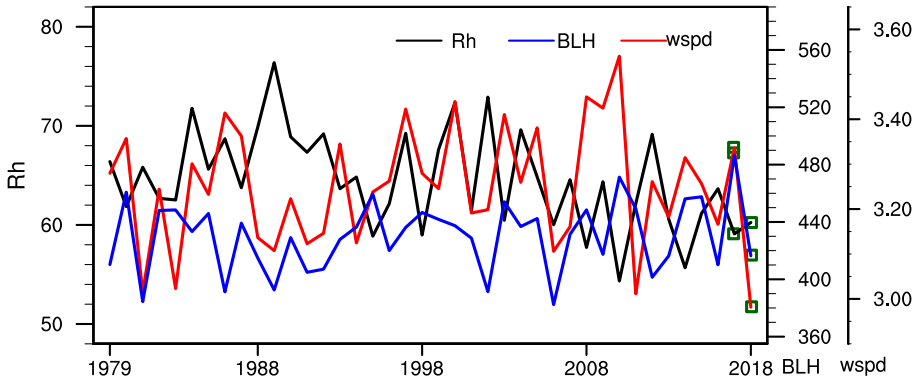

Fig. 4. Variations in winter-mean surface relative humidity (black, unit: %), BLH (blue, unit: m) and surface wind speed (red, unit: m/s) from 1979 to 2018 in the 2 + 26 region. The green rectangles indicate the variables in 2017 and 2018.

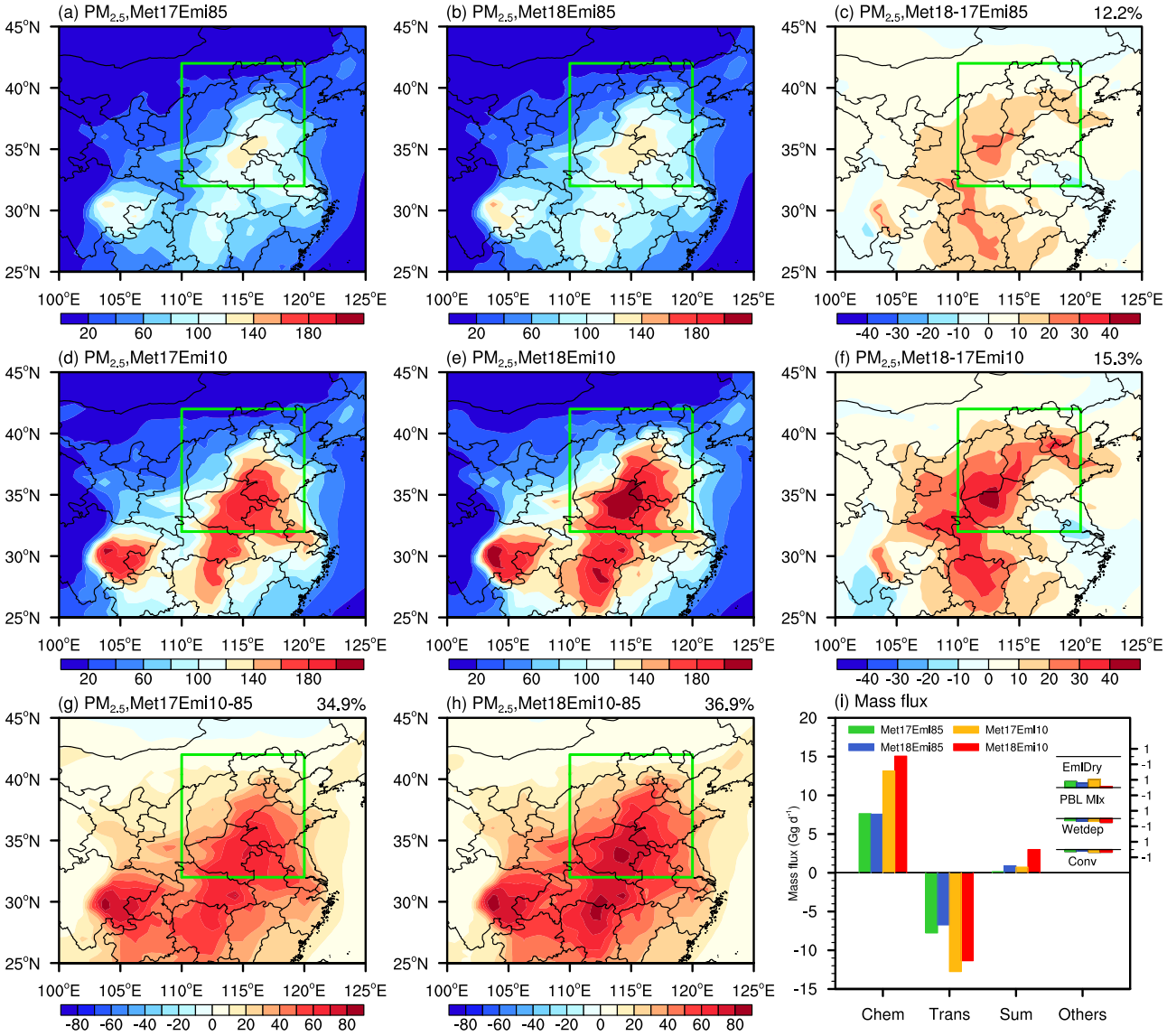

Fig. 5. The concentrations of $PM_{2.5}$ (unit: μg m^{-3}) simulated by GEOS-Chem model in experiments named Met17Emi85 (a), Met18Emi85 (b), Met17Emi10 (d) and Met18Emi10 (e). The $PM_{2.5}$ differences (unit: μg m^{-3}) resulted from meteorological conditions (fixed emissions) under emission in 1985 (c, Met18Emi85 – Met17Emi85), and emission in 2010 (d, Met18Emi10 – Met17Emi10). The increased proportion on panel c, f calculated as $PM_{2.5}$ differences/($PM_{2.5}$ in 2018 + $PM_{2.5}$ in 2017), where the $PM_{2.5}$ concentrations were averaged on the 2 + 26 region. The $PM_{2.5}$ differences (unit: μg m^{-3}) resulted from various emissions (fixed meteorological conditions) under meteorological conditions in 2017 (g, Met17Emi10 – Met17Emi85), and meteorological conditions in 2018 (h, Met18Emi10 – Met18Emi85). The increased proportion on panel g, h calculated as $PM_{2.5}$ differences/$PM_{2.5}$ from emission 2010, where the $PM_{2.5}$ concentrations were averaged on the 2 + 26 region. (i) Winter mean mass fluxes of aerosols (bottom axis: chemistry reaction, convection, emissions+dry deposition, wet deposition, PBL mixing, transport and their sums, unit: Gg d^{-1}) in the 2 + 26 region. The mass fluxes were calculated within the planetary boundary layer and as the sum of sulfate, nitrate, ammonium, black carbon, and organic carbon. The green box is the location of the 2 + 26 region.

existence of anomalous anticyclonic circulations over North China. On the upper troposphere, the East Asia jet stream was weaker in 2018 than in 2017, which was shown by negative anomalies in the zonal wind at 200 hPa and indicated weak cold air intensity in the north of China (Fig. 6a). Modulated by such atmospheric circulations, the horizontal dispersion (indicated by surface wind speed, Fig. 3b) and vertical exchange (represented by BLH, Fig. 3a) were both favourable for the occurrence of haze pollution (high $PM_{2.5}$ concentrations, Fig. 1c) in the winter of 2018.

The aforesaid large-scale atmospheric circulations and local meteorological conditions were the simultaneous climate factors responsible for differences in winter haze pollution between 2018 and 2017. The question arises whether we can identify several preceding climate factors, which contributed to the number of winter haze days in the 2 + 26 region (HD_{226}). As reported by Yin et al. (2019), winter haze on the North China Plain showed a positive relationship with the preceding autumn sea ice on the Beaufort Sea (correlation coefficient with HD_{226} = 0.38 during 1979–2016, above 99% confidence level, Fig. S3a). Associated with positive sea ice anomalies, anomalous atmospheric circulation resembled the positive phase of the EA/WR and EU patterns (Fig. S3b). According to the results of Yin et al. (2019), these positive sea ice anomalies in Beaufort Sea (2018 minus 2017, Fig. 6b) should trigger anomalous teleconnection patterns and finally induce favourable environments for higher $PM_{2.5}$ concentrations in 2018 (Fig. 1c).

The North Atlantic Oscillation combines parts of the EA/WR patterns, which was one of the dominant modes of variability over the North Atlantic (Barnston and Livezey, 1987). The SST anomalies, associated with the NAO pattern, showed a “triple pattern” in the north Atlantic (Trenberth et al., 2019). The negative SST anomalies in the tropical and high-latitude Atlantic regions (Fig. S3c) had close relationships with enhanced winter haze in China (correlation coefficient with

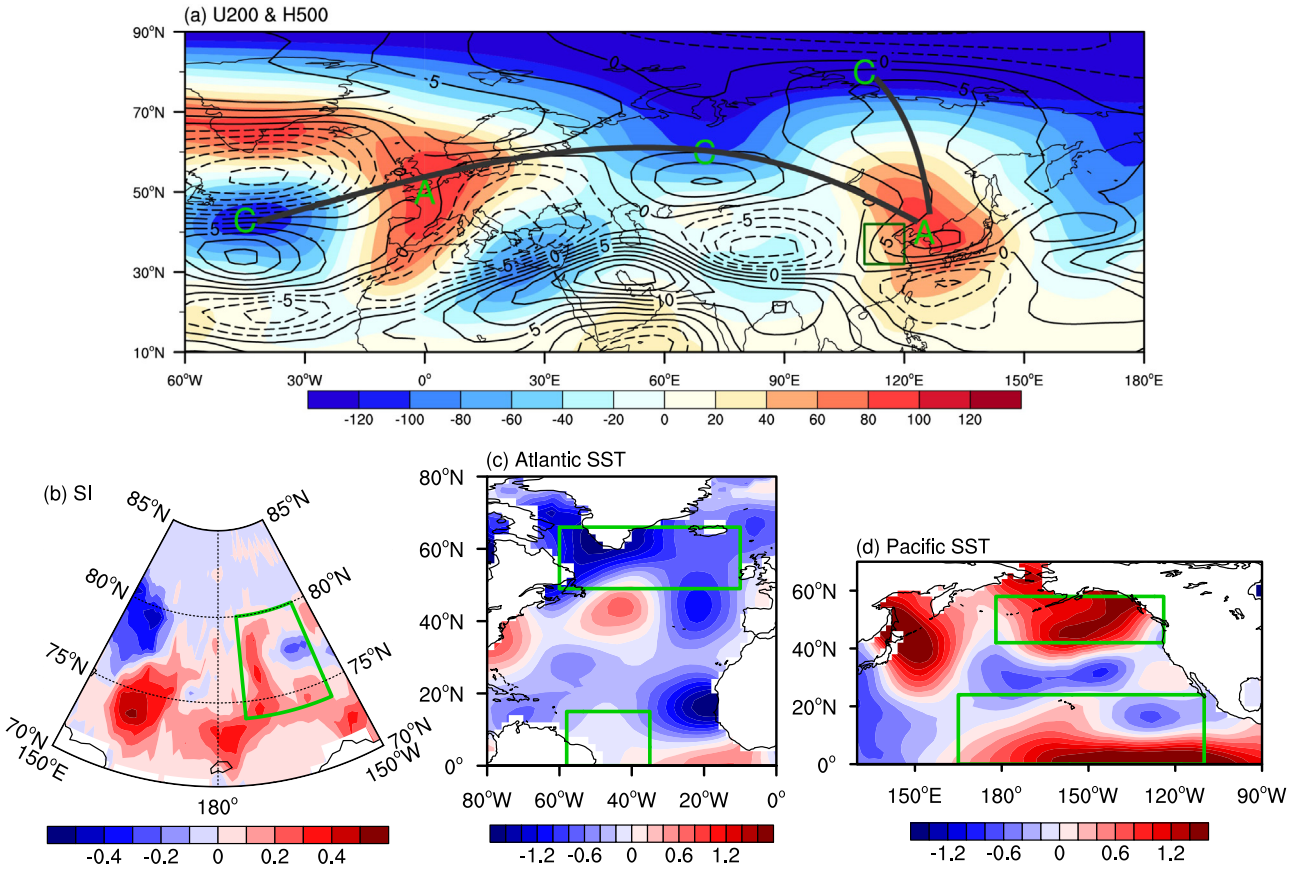

Fig. 6. Differences of (a) winter zonal wind at 200 hPa (contour, unit: m/s), H500 (shading, unit: gpm) between 2018 and 2017 (2018 minus 2017). The green box is the location of the 2 + 26 region. Differences of preceding Arctic sea ice concentrations (b, %), Atlantic SST (c, °C) and Pacific SST (d, °C) between 2018 and 2017. In panel b, the area-mean sea ice in the green box (74–80°N, 155–175°W) was calculated and designated the ASI_B index. In panel c, the area-mean SST in the green boxes (0–16°N, 32–58°W; 49–66°N, 10–60°W) was calculated as the SST_A index. In panel d, the area-mean SST in the green boxes (0–24°N, 165°E–110°W; 42–58°N, 178°E–124°W) was calculated and designated the SST_P index.

HD_{226} = 0.65) via inducing a meridional pattern in the upper troposphere which then propagated zonally through Eurasia to North China and reduced the frequency of cold air (Xiao et al., 2015, Fig. S3d). Compared to that in 2017, the SST in the autumn of 2018 was cooler in the lower and higher latitudes but was slightly warmer in the mid-latitudes (Fig. 6c), showing the "triple pattern" and contributing to high $PM_{2.5}$ concentrations in the winter of 2018 (Fig. 1c).

In the north of Pacific, the SST differences between the winters of 2018 and 2017 also showed a clear "triple pattern", consisting of positive SST anomalies over the Gulf of Alaska and Central-east Pacific and negative anomalies over northwestern Pacific (Fig. 6d). This "triple pattern" of SST anomalies (correlation coefficient with HD_{226} = −0.50, Fig. S3e) significantly resulted in severe winter haze pollution in North China in the autumns of 2013 and 2014, and related to lowest HD_{226} in 2010 (Yin and Wang, 2016, Yin and Wang, 2017). The induced atmospheric anomalies (Fig. S3f) were similar to those in Fig. 6a, whose key features were the positive phase of EA/WR and EU patterns and stronger anticyclonic circulations. It is well-reasoned that the positive "triple pattern" Pacific SST anomalies in winter 2018 (Fig. 6d) might resulted in the teleconnection pattern (i.e., EA/WR and EU positive phase) and local atmospheric circulations (i.e., anomalous anticyclone) that intensified the haze pollution in the 2 + 26 region (Fig. 1c).

6. Conclusions and discussion

Since 2013, strict air pollution control effectively contributed to the trend of decreasing in $PM_{2.5}$ in China. To consolidate the managing effects, intensified air pollution preventions were strictly implemented in the "2 + 26" cities during the winters of 2017 and 2018. This regional pollution policy was intended to more effectively reduce $PM_{2.5}$ concentrations in the Beijing-Tianjin-Hebei region (Chen et al., 2019), however, the $PM_{2.5}$ concentrations in the 2 + 26 region exhibited severe rebound in 2018. Comparing 2018 and 2017 (2018 minus 2017), sea ice concentrations in the west Beaufort Sea showed positive anomalies. There were "triple pattern" SST anomalies in both the North Pacific and North Atlantic. These anomalous external factors stimulated teleconnection patterns such as a positive phase in the EA/WR and EU patterns and finally enhanced anomalous anticyclonic circulations over the 226 region. Thus, the local surface wind speeds were reduced by anomalous surface southerlies, indicating limited horizontal dispersion conditions. In addition, conditions in the lower boundary layer were favourable for the accumulation of particulates. However, the differences in moisture conditions in these two years were negligible, therefore, were not one of the reasons for the observed in $PM_{2.5}$ rebound. To enhance the signals in the atmosphere, the differences between 2018 and 2017 were analysed in the main text (Fig. 3, 6a). It is notable that the anomalies in 2017 and 2018, relative to the mean of 2014–2018, illustrated well-agreed features (Fig. S4). The observational analyses on the impacts of meteorological anomalies were verified by the results of GEOS-Chem simulations. The simulated $PM_{2.5}$ concentrations (with fixed emissions) driven by meteorology in 2018 were 12–15% higher than those with atmospheric circulations in 2017, close to the observed 10% $PM_{2.5}$ rebound. The process analysis illustrated that the stagnated air weakened the outflow of pollutant particles but enhanced the chemical reactions to produce more secondary aerosols, and thus held more aerosol particles in 2 + 26 region.

As mentioned in Section 4, it is better to evaluate the real emissions in the winter 2017 and 208 and to drive the GEOS-Chem model with

them, however, our study was limited by generally delayed update of emission inventory. Alternatively, we fixed the emissions both at a high (2010) and low (1985) level and drove the GEOS-Chem model solely with varied atmospheric circulations in 2017 and 2018. These experiments could fix the impacts of the anthropogenic emissions, and the results strongly confirmed the impacts of meteorology on the rebound of haze pollution in winter 2018. Indeed, there were still gaps to understand the real joint effects of meteorology and human activities in 2017 and 2018, thus, further studies should import the updated emissions inventory in these two winters into the simulations.

The $PM_{2.5}$ emissions in 1985 were lowest since 1985 (Fig. S1c), while those in 2010 approached the highest point (Dang and Liao, 2019). Reducing the emissions from the level in 2010 to that in 1985 meant ideally super-strong pollution regulations. As expected, the $PM_{2.5}$ reduced approximately 34.9–36.9% relative to the simulations driven by emissions in 2010 (Fig. 5g, h). The $PM_{2.5}$ differences under the atmospheric circulations in 2018 (Met18Emi10 - Met18Emi85, Fig. 5h) were larger than those modulated by the meteorological conditions in 2017 (Fig. 5g). The meteorological conditions not only had impacts on the $PM_{2.5}$ concentrations but also influenced the effects of the emission reductions, which jointly resulted in 12.2% higher $PM_{2.5}$ by the stagnated atmospheric circulations than those under good ventilation conditions even under same emission reductions (Fig. 5a, b). The daily bad (good) dispersion conditions were separated according to the observed $PM_{2.5} > 100\ \mu g\ m^{-3}$ ($<75\ \mu g\ m^{-3}$). The decrements, due to emission reducing from the level in 2010 to that in 1985, were also calculated during these two kind of dispersion conditions. The daily-mean decrements of $PM_{2.5}$ concentrations was ~60 $\mu g\ m^{-3}$ under bad ventilation conditions and ~20 $\mu g\ m^{-3}$ with dispersed atmosphere, respectively (Fig. 7a). Here, we can treat the experiments driven by meteorology in 2017 and 2018 as two annual cases. The total effects of emission reductions (i.e., the sum decrease of $PM_{2.5}$ shifting from the emissions in 2010 to 1985) were 3085 $\mu g\ m^{-3}$ in 2017. Although the number of days with bad dispersion conditions were only 26 days, the emission reductions contributed about 50% of the total $PM_{2.5}$ decrease in 2017 (Fig. 7b). The emission reductions with good dispersions were implemented in 46 days and only resulted in 30% of the total $PM_{2.5}$ decrease (Fig. 7b). The sum decrease of $PM_{2.5}$ was 3806 $\mu g\ m^{-3}$ in 2018. The emission reductions under stagnated (dispersed) atmosphere were carried out in 32 (34) days and resulted in 53% (21%) of the total $PM_{2.5}$ decrease in 2018 (Fig. 7b). The efficiency of emission reduction was much higher in the stagnated weather than that in the dispersed days. This implied that, highly cost effective measures should be launched and executed depending on accurate hazy weather forecast 3–7 days ahead. Furthermore, when the wintertime atmospheric circulations were predicted to be stagnant 1–3 months in advance, look-ahead strengthened emission reductions must be planned to offset the effects of adverse climate conditions (Wang, 2018).

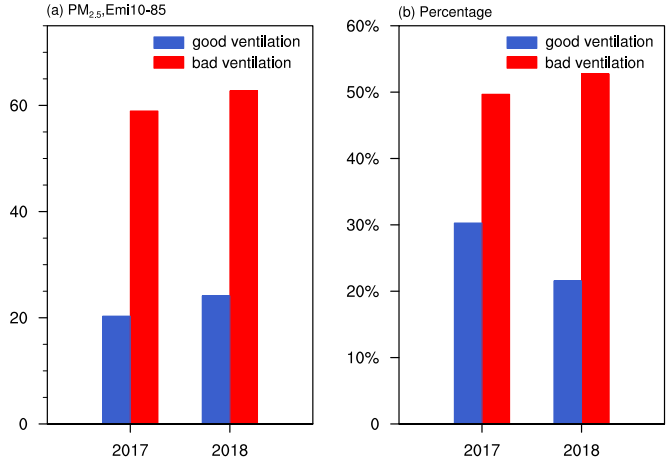

Fig. 7. (a) Daily-mean difference of $PM_{2.5}$ concentrations (unit: $\mu g\ m^{-3}$) between simulations driven by emission of 2010 and 1985 under good (blue) and bad (good) ventilation conditions. (b) Percentage $PM_{2.5}$ decrease under good (blue) and bad (good) ventilation conditions (relative to the yearly total $PM_{2.5}$ decrease). The good (bad) ventilation conditions were defined as the observed $PM_{2.5} < 75\ \mu g\ m^{-3}$ ($>100\ \mu g\ m^{-3}$).

CRediT authorship contribution statement

Zhicong Yin: Conceptualization, Validation, Writing - original draft, Visualization, Project administration, Funding acquisition.**Yijia Zhang:** Software, Data curation.

Declaration of competing interest

The authors declare no conflict of interest.

Acknowledgements

The China National Key Research and Development Plan Project (2016YFA0600703), National Natural Science Foundation of China (41705058, 41991283 and 91744311), and the funding of Jiangsu Innovation & Entrepreneurship team supported this research.

Authors' contribution

Yin Z. C. designed the research. Yin Z. C. and Zhang Y. J. performed research. Yin Z. C. prepared the manuscript with contributions from all co-authors.

Appendix A. Supplementary data

Supplementary data to this article can be found online at https://doi.org/10.1016/j.scitotenv.2020.138514.

References

An, Z.S., Huang, R.L., Zhang, R.Y., Tie, X.X., Li, G.L., Cao, J.L., Zhou, W.J., Shi, Z.G., Han, Y.M., Gu, Z.L., Ji, Y.M., 2019. Severe haze in northern China: a synergy of anthropogenic emissions and atmospheric processes. P NATL ACAD SCI USA 116, 8657–8666.

Barnston, A.G., Livezey, R.E., 1987. Classification, seasonality and persistence of low frequency atmospheric circulation patterns. Mon. Wea. Rev. 115, 1083–1126.

Bey, I., Jacob, D.J., Yantosca, R.M., Logan, J.A., Field, B.D., Fiore, A.M., Li, Q.B., Liu, H.G.Y., Mickley, L.J., Schultz, M.G., 2001. Global modeling of tropospheric chemistry with assimilated meteorology: model description and evaluation. J. Geophys. Res.-Atmos. 106, 23073–23095. https://doi.org/10.1029/2001jd000807.

Chen, H., Wang, H., 2015. Haze days in North China and the associated atmospheric circulations based on daily visibility data from 1960 to 2012. J. Geophys. Res. Atmos. 120, 5895–5909. https://doi.org/10.1002/2015JD023225.

Chen, Z., Chen, D., Wen, W., Zhuang, Y., Kwan, M.-P., Chen, B., Zhao, B., Yang, L., Gao, B., Li, R., Xu, B., 2019. Evaluating the "2+26" regional strategy for air quality improvement during two air pollution alerts in Beijing: variations in PM2.5 concentrations, source apportionment, and the relative contribution of local emission and regional transport. Atmos. Chem. Phys. 19, 6879–6891. https://doi.org/10.5194/acp-19-6879-2019.

Dang, R., Liao, H., 2019. Severe winter haze days in the Beijing–Tianjin–Hebei region from 1985 to 2017 and the roles of anthropogenic emissions and meteorology. Atmos. Chem. Phys. 19, 10801–10816. https://doi.org/10.5194/acp-19-10801-2019.

Dee, D.P., Uppala, S.M., Simmons, A.J., Berrisford, P., Poli, P., Kobayashi, S., Andrae, U., Balmaseda, M.A., Balsamo, G., Bauer, P., Bechtold, P., Beljaars, A.C.M., 2011. The ERA interim reanalysis: configuration and performance of the data assimilation system. Q. J. Roy. Meteor. Soc. 137, 553–597. https://doi.org/10.1002/qj.828.

Ding, Y., Liu, Y., 2014. Analysis of long-term variations of fog and haze in China in recent 50 years and their relations with atmospheric humidity. Science China Earth Sciences 57, 36–46. https://doi.org/10.1007/s11430-013-4792-1.

Feng, J., Li, J., Liao, H., Zhu, J., 2019. Simulated coordinated impacts of the NAO and El Niño on aerosol concentrations over eastern China. Atmos. Chem. Phys. 19, 10787–10800. https://doi.org/10.5194/acp-19-10787-2019.

Gelaro, R., McCarty, W., Suarez, M.J., Todling, R., Molod, A., Takacs, L., Randles, C.A., Darmenov, A., Bosilovich, M.G., Reichle, R., Wargan, K., Coy, L., Cullather, R., Draper, C., Akella, S., Buchard, V., Conaty, A., da Silva, A.M., Gu, W., Kim, G.K., Koster, R., Lucchesi, R., Merkova, D., Nielsen, J.E., Partyka, G., Pawson, S., Putman, W., Rienecker, M., Schubert, S.D., Sienkiewicz, M., Zhao, B., 2017. The modern-era retrospective analysis for research and applications, version 2 (MERRA-2). J. Clim. 30, 5419–5454. https://doi.org/10.1175/jcli-d-16-0758.1.

He, J.J., Gong, S.L., Zhou, C.H., Lu, S.H., Wu, Lin., Chen, Y., Yu, Y., Zhao, S.P., Yu, L.J., Yin, C.M., 2018. Analyses of winter circulation types and their impacts on haze pollution in Beijing. Atmos. Environ. 192, 94–103.

Kalnay, E., Kanamitsu, M., Kistler, R., Collins, W., Deaven, D., Gandin, L., Iredell, M., Saha, S., White, G., Woollen, J., Zhu, Y., Leetmaa, A., Reynolds, R., Chelliah, M., Ebisuzaki, W., Higgins, W., Janowiak, J., Mo, K.C., Ropelewski, C., Wang, J., Jenne, R., Joseph, D., 1996. The NCEP/NCAR 40-year reanalysis project. B. Am. Meteorol. Soc. 77, 437–471. https://doi.org/10.1175/1520-0477(1996)077<0437:TNYRP>2.0.CO;2.

Li, K., Jacob, D.J., Liao, H., Shen, L., Zhang, Q., Bates, K.H., 2019. Anthropogenic drivers of 2013–2017 trends in summer surface ozone in China. P NATL ACAD SCI USA 116, 422–427. https://doi.org/10.1073/pnas.1812168116.

Liu, D., Yan, W., Kang, Z., Liu, A., Zhu, Y., 2018. Boundary-layer features and regional transport process of an extreme haze pollution event in Nanjing, China. Atmos. Pollut. Res. 9, 1088–1099.

Ma, X.H., Liao, X.N., Tang, Y.X., Sun, Z.B., Li, Z.M., 2017. Weather pattern and cause analysis of air heavy pollution days in Beijing. J. Meteorol. Environ. 33 (5), 53–60 (in Chinese).

Park, R.J., Jacob, D.J., Field, B.D., Yantosca, R.M., Chin, M., 2004. Natural and transboundary pollution influences on sulfate-nitrate-ammonium aerosols in the United States: implications for policy. J. Geophys. Res.-Atmos. 109, D15204. https://doi.org/10.1029/2003jd004473.

Rayner, N.A., Parker, D.E., Horton, E.B., Folland, C.K., Alexander, L.V., Rowell, D.P., Kent, E.C., Kaplan, A., 2003. Global analyses of sea surface temperature, sea ice, and night marine air temperature since the late nineteenth century. J. Geophys. Res. 108 (14), 4407. https://doi.org/10.1029/2002JD002670.

Shi, P.J., Zhang, G.F., Kong, F., Chen, D.L., Azorin-Molina, Cesar, Guijarro, Jose A., 2019. Variability of winter haze over the Beijing-Tianjin-Hebei region tied to wind speed in the lower troposphere and particulate sources. Atmos. Res. 215, 1–11.

Smith, T., Reynolds, R., Peterson, T., Lawrimore, J., 2008. Improvements to NOAA's historical merged land-ocean surface temperature analysis (1880–2006). J. Clim. 21, 2283–2296.

Trenberth, Kevin, Zhang, Rong, National Center for Atmospheric Research Staff, 2019. The Climate Data Guide: Atlantic Multi-decadal Oscillation (AMO). https://climatedataguide.ucar.edu/climate-data/atlantic-multi-decadal-oscillation-amo, Accessed date: 10 January 2019.

Wang, H.J., 2018. On assessing haze attribution and control measures in China. Atmos. Oceanic Sci. Lett. 11, 120–122. https://doi.org/10.1080/16742834.2018.1409067.

Wang, H.J., Chen, H.P., Liu, J.P., 2015. Arctic Sea ice decline intensified haze pollution in eastern China. Atmos. Oceanic Sci. Lett. 8, 1–9. https://doi.org/10.3878/AOSL20140081.

Xiao, D., Li, Y., Fan, S., Zhang, R., Sun, J., Wang, Y., 2015. Plausible influence of Atlantic Ocean SST anomalies on winter haze in China. Theor. Appl. Climatol. 122, 249–257. https://doi.org/10.1007/s00704-014-1297-6.

Yin, Z., Wang, H., 2016. The relationship between the subtropical Western Pacific SST and haze over north-central North China plain. Int. J. Climatol. 36, 3479–3491. https://doi.org/10.1002/joc.4570.

Yin, Z., Wang, H., 2017. Role of atmospheric circulations in haze pollution in December 2016. Atmos. Chem. Phys. 17, 11673–11681. https://doi.org/10.5194/acp-17-11673-2017.

Yin, Z., Wang, H., Chen, H., 2017. Understanding severe winter haze events in the North China plain in 2014: roles of climate anomalies. Atmos. Chem. Phys. 17, 1641–1651. https://doi.org/10.5194/acp-17-1641-2017.

Yin, Z., Li, Y., Wang, H., 2019. Response of early winter haze days in the North China plain to autumn Beaufort Sea ice. Atmos. Chem. Phys. 19, 1439–1453.

Yin, Z.C., Wang, H.J., Guo, W.L., 2015. Climatic change features of fog and haze in winter over North China and Huang-Huai area. Sci. China Earth Sci. 58, 1370–1376.

Zhang, Z., Gong, D., Mao, R., Qiao, L., Kim, S.J., Liu, S., 2019. Possible influence of the Antarctic oscillation on haze pollution in North China. J. Geophys. Res. Atmos. 124, 1307–1321. https://doi.org/10.1029/2018JD029239.

Zhong, W.G., Yin, Z.C., Wang, H.J., 2019. The relationship between the Anticyclonic anomalies in Northeast Asia and severe haze in the Beijing–Tianjin–Hebei region. Atmos. Chem. Phys. 19, 5941–5957. https://doi.org/10.5194/acp-19-5941-2019.